Steel and Composite Structures, Vol. 9, No. 3 (2009) 255-274
DOI: http://dx.doi.org/10.12989/scs.2009.9.3.255

Light-gauge composite floor beam with self-drilling screw shear connector: experimental study

Szilvia Erdélyi

Department of Structural Mechanics, Budapest University of Technology and Economics, Hungary

László Dunai*

Department of Structural Engineering, Budapest University of Technology and Economics, Hungary

(Received April 10, 2006, Accepted February 19, 2009)

Abstract. This paper presents an experimental study of a newly developed composite floor system, built up from thin-walled C-profiles and upper concrete deck. Trapezoidal sheeting provides the formwork and the fastening of the sheet transmits the shear forces between the C-profiles and the deck. The modified formation of the standard self-drilling screw in the beam-to-sheet connection is applied as shear connector. Push-out tests are completed to study the composite behaviour of the different connection arrangements. On the basis of the test results the behaviour is characterized by the observed failure modes. The design values of the connection stiffness and strength are calculated by the recommendation of Eurocode 4. In the next phase of the experimental study six full-scale composite beams are tested. The global geometry is based on the proposed geometry of the developed floor system. The applied shear connections are selected as the most efficient arrangements obtained from the push-out tests. The experimental behaviour of the composite beams are discussed and evaluated. As a conclusion of the experimental study the Eurocode 4 plastic design method is validated for the developed composite floor.

Keywords : light-gauge composite floor; self-drilling screw; push-out test; full-scale beam test; failure modes; relative slip; design values.

1. Introduction

In residential steel buildings the floor system in general is built by a framing of thin-walled joist and an upper deck. The floor deck is solved by "dry" or "wet" technology. In case of "dry" technology usually a wood based plate system is fastened to the beams. The composite action between the beams and the floor deck has a low degree (generally neglected in design) so that the span of the floor is limited by the load bearing capacity and stiffness of the thin-walled beams.

The "wet" technology is more complicated to erect but it has several advantages. On the top of the thin-walled beam framing a thin concrete deck is placed with the application of trapezoidal sheeting or plywood as a formwork. The composite action between the thin-walled profiles and the concrete deck is provided by special mechanical, non-welded shear connectors which are formed according to the

* Corresponding Author, Email: ldunai@epito.bme.hu

structural characteristics of thin-walled cold-formed structures. Generally the modified formation of common connector elements in beam-to-sheet connection - the self-drilling or self-tapping screw - or other special profile or channel elements are used. By the application of an efficient shear connection between the steel framing and the concrete deck the composite action can reach the required degree to be applied in practical cases. The application of concrete improves the dynamic behaviour of the floor, too.

Recently a composite light-gauge floor system - called LindabFloor - was developed by the co-operation of the Department of Structural Engineering, Budapest University of Technology and Economics (BME), and Lindab Profile Ltd, Hungary. The framing of the system is built by thin-walled, cold-formed C-profiles, and the concrete deck is installed on trapezoidal sheeting as a formwork. The composite action is solved by partially drilled self-drilling screw beam-to-sheet connections.

To determine the behaviour and efficiency of this type of shear connection an extended parametric push-out test programme is designed and completed. On the basis of the pilot test results (Erdélyi and Dunai 2002) a proper connection type was chosen for the application in LindabFloor structures and additional tests were done with further parameters (Erdélyi and Dunai 2004). Finally a total of 42 specimens were investigated.

Based on the push-out test results the design values of the connections (stiffness, resistance and ductility) were determined (Erdélyi and Dunai 2004). By the consideration of the behaviour and design aspects of thin-walled structures and the observed low stiffness of the shear connection, a new design procedure of composite light-gauge beam was developed (Dunai, *et al*. 2003/a) and design tables were determined (Dunai, *et al*. 2003/b) according to the recommendations of the Eurocode 3, Part 1-3 and the Eurocode 4.

In the next phase of the research six full-scale light-gauge composite floor beams were tested. The structural arrangement of the beams was derived on the basis of the developed floor system. The global geometry of the floor beams were the same, the effect of the thickness of the C-profile, the arrangement of the trapezoidal sheeting and different shear connections - in accordance with the results of the push-out tests - were investigated. The stiffness, the ultimate behaviour and the composite action of the beams were studied. The test results were compared and verified by the resistance values of the proposed design method (Erdélyi 2007).

2. Background of new system development

2.1 Existing systems

In general the framing of light-gauge composite floor systems is built by thin-walled, cold-formed C- or Z-profiles, as it is illustrated in Fig. 1/a. An alternative solution for large spans, the truss system is also used.

The applied height of the joist is determined by the whole thickness of the floor structure and the local buckling phenomenon of the thin-walled profile. Consequently the height generally ranges from 150 to 250 mm, with 1,5 to 2,5 mm nominal thickness. The typical distance between the floor beams is 600 mm. During the construction of the floor light-gauge profiles or other bracing system provides with the lateral support. After the construction is completed the concrete deck for the upper flange while hat profiles and fastened gypsum boards for bottom flange ensure the lateral support, as shown in Fig.1/a.

The formwork of the concrete deck is plywood or trapezoidal sheeting. When plywood is applied the bottom side of the deck keeps plane and the formwork can be removed after concreting. The other solution is the trapezoidal sheeting as a permanent formwork. In this case the composite action between

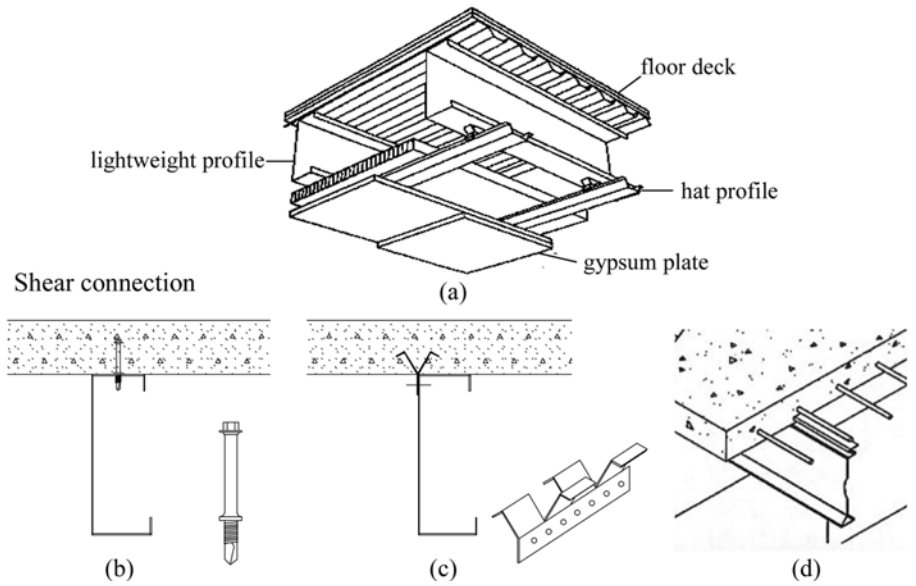

Fig. 1 a) General light-gauge floor geometry, b) Standoff screw, c) MSC shear connector, d) Embedded profile

the deck and the C-profile is provided by the fastening of the sheeting to the top flange of the C-profile. The concrete fill in the rib and the shear connector inside and after the hardening the forces are transmitted between the steel framing and the deck. The thickness of the concrete deck ranges from 50 to 80 mm (above the rib, if exist).

The shear connectors are non-welded, mechanical components. Three main types of solutions are applied: a) the shear connector is a common self-drilling screw in modified formation b) special profile element, fastened to the C-section or cut out and bent up from the flanges, or c) the whole top flange of the beam profile embeds into the concrete. Figs. 1/b-d show examples for the different detailing.

The standoff screw (Mujagic, *et al.* 2001) is a modified self-drilling and self-tapping screw, manufactured with a special, variable length standoff shank that stops the drilling when the adequate embedment in the concrete is reached, as it is illustrated in Fig. 1/b. It is a promising alternative for the welded headed studs in short-span composite floors, developed also for hot rolled sections and thin-walled beams. Fig. 1/c shows a special, V-profile element with a continuous, longitudinal web strip, called Metal Stud Crete (MSC) connector (Earl Composite Systems 2001). The longitudinal strip is fastened to the top flange or to the web depending on the structural arrangement. This shear connector is developed for wall panels but can be used in floors, too.

The embedded profile is illustrated in Fig. 1/d: the upper part of a special cold-formed joist is placed into the concrete without application of any shear connector (Building Works, Inc. 2003). The reinforcing material is welded to the deformed edge.

Several other types of profiled shear connectors are presented and investigated by push-out and full-scale beam tests (Hanaor 2000).

2.2 Structural arrangement of the developed system

The developed light-gauge composite floor system is built by thin-walled cold-formed C-profile, as it

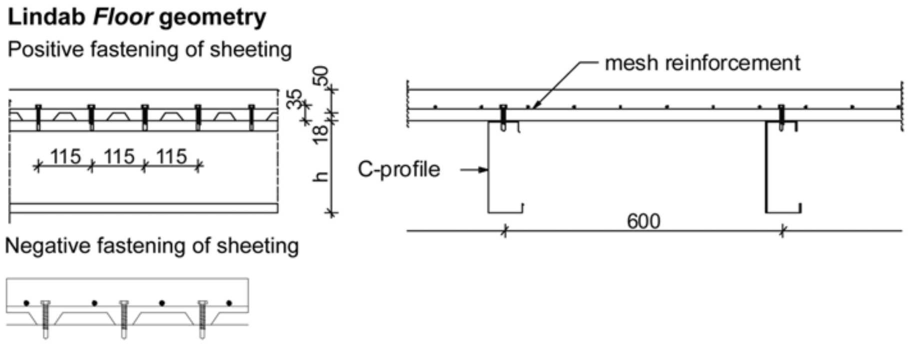

Fig. 2 Structural arrangement of the developed composite floor

is illustrated in Fig. 2. The height of the joists ranges from 150 to 250 mm, with 1,5 to 2,5 mm nominal thickness. The composite action is provided by the beam-to-sheet connection, using the common self-drilling screw what is drilled partially; the head and the threaded part - embedded in concrete - act as shear connector. The formwork is permanent trapezoidal sheet with 18 mm height and 0,5 mm nominal thickness (LTP20). Fig. 2 shows the deck geometry formed by the two possible fastening mode of LTP20 trapezoidal sheeting. Since the two arrangements are quite different in the zone of the shear connection, both of them is investigated by test.

3. Push-out tests on shear connectors

3.1 Experimental programme

The experimental arrangement and the test specimens are shown in Fig. 3. The geometry of the specimens is designed according to Eurocode 4 recommendations with the pertinent changes due to the

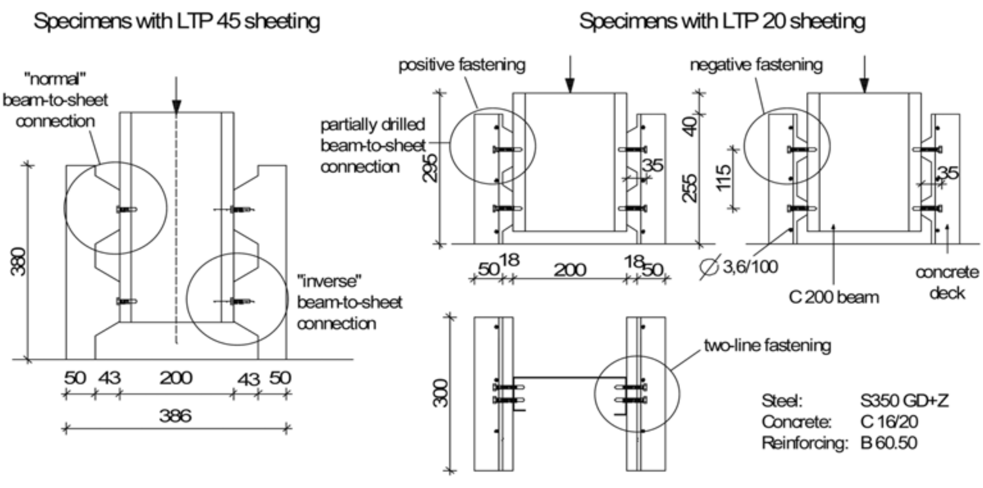

Fig. 3 Geometry of the push-out specimens

structural characteristics. Two connections are placed in both sides of the C-profile; the distance between the screws is determined by the waves of sheeting.

The parameters of the different specimens can be seen in Table 1. In the first series of experiments (12 specimens) the efficiency of the different screws and their fastening modes are studied. In the next phase a parametric study is completed with 30 specimens, based on the previous results and the final geometry of the developed floor system. The efficient connection forms are investigated with the following main parameters of the components: the screw type and geometry, the embedment depth, the trapezoidal sheeting arrangement, the thickness of the C-profile and the existence of the reinforcement. The last 12

Table 1 Parameters of push-out specimens

No.	*Notations experiments #1*	*Screw*				$t_{C\text{-profile}}$ *[mm]*	*Sheet*		*Rein-forc.*	*Sp.*
		type-diam.	*fast. mode*	*scr. line*	*emb. [mm]*		*type-thickn.*	*fast.*		
1	SDn-1-s5	SD6-6.3	norm.	1	-	1,5	LTP45-0.5	pos	no	1
2	SDn-1-s7	SD6-6.3	norm.	1	-	1,5	LTP45-0.7	pos	no	1
3	SDi-1-30-s7	SD6-6.3	inv.	1	30	1,5	LTP45-0.7	pos	no	1
4	SDi-2-30-s7	SD6-6.3	inv.	2	30	1,5	LTP45-0.7	pos	no	1
5	HS-1-30-s5	HS-6.3	part.	1	30	1,5	LTP45-0.5	pos	no	1
6	HS-1-30-s7	HS-6.3	part.	1	30	1,5	LTP45-0.7	pos	no	1
7	HS-1-45-s5	HS-6.3	part.	1	45	1,5	LTP45-0.5	pos	no	1
8	HS-1-60-s5	HS-6.3	part.	1	60	1,5	LTP45-0.5	pos	no	1
9	HS-2-30-s5	HS-6.3	part.	2	30	1,5	LTP45-0.5	pos	no	1
10	HS-2-60-s5	HS-6.3	part.	2	60	1,5	LTP45-0.5	pos	no	1
11	SXC-1-45-s5	SXC5-5.5	part.	1	45	1,5	LTP45-0.5	pos	no	1
12	SXC-1-55-s5	SXC5-5.5	part.	1	55	1,5	LTP45-0.5	pos	no	1
13	EJ-1-t1.5-sp	EJOT-6.3	part.	1	35	1,5	LTP20-0.5	pos	no	2
14	EJ-1-t1.5-sn	EJOT-6.3	part.	1	35	1,5	LTP20-0.5	neg	no	2
15	EJ-2-t1.5-sp	EJOT-6.3	part.	2	35	1,5	LTP20-0.5	pos	no	1
16	EJ-2-t1.5-sn	EJOT-6.3	part.	2	35	1,5	LTP20-0.5	neg	no	1
17	EJ-1-t2.0-sp	EJOT-6.3	part.	1	35	2,0	LTP20-0.5	pos	no	2
18	EJ-1-t2.0-sn	EJOT-6.3	part.	1	35	2,0	LTP20-0.5	neg	no	2
19	EJ-2-t2.0-sp	EJOT-6.3	part.	2	35	2,0	LTP20-0.5	pos	no	1
20	EJ-2-t2.0-sn	EJOT-6.3	part.	2	35	2,0	LTP20-0.5	neg	no	1
21	EJ-1-t2.5-sp	EJOT-6.3	part.	1	35	2,5	LTP20-0.5	pos	no	2
22	EJ-1-t2.5-sn	EJOT-6.3	part.	1	35	2,5	LTP20-0.5	neg	no	2
23	EJ-2-t2.5-sp	EJOT-6.3	part.	2	35	2,5	LTP20-0.5	pos	no	1
24	EJ-2-t2.5-sn	EJOT-6.3	part.	2	35	2,5	LTP20-0.5	neg	no	1
25	EJ-1-t1.5-sp-rf	EJOT-6.3	part.	1	35	1,5	LTP20-0.5	pos	yes	2
26	EJ-1-t2.0-sp-rf	EJOT-6.3	part.	1	35	2,0	LTP20-0.5	pos	yes	2
27	EJ-1-t2.0-sn-rf	EJOT-6.3	part.	1	35	2,0	LTP20-0.5	neg	yes	2
28	EJ-1-t2.5-sp-rf	EJOT-6.3	part.	1	35	2,5	LTP20-0.5	pos	yes	2
29	SX1-t2.0-sp-rf	SXC5-5.5	part.	1	35	2,0	LTP20-0.5	pos	yes	2
30	SX2-t2.0-sp-rf	SXC5-5.5	part.	2	35	2,0	LTP20-0.5	pos	yes	2

specimens are investigated in parallel with the pertinent full-scale beam tests (to be discussed in Section 4). In several cases two equivalent specimens are tested with the same geometry, as it is noted in Table 1. Consequently the amount of different specimens is 30, as Table 2 shows.

In the first series of specimens trapezoidal sheeting with 45 mm depth is applied (LTP45) that resulted bigger ribs and almost 100 mm thickness of concrete (43 mm rib + 50 mm plate), as Fig. 3 shows. In order to reduce the height of the concrete deck and the structural depth of the floor, in the final arrangement the sheet with 18 mm depth was used (LTP20). The positive and negative fastening mode of the LTP20 sheeting is quite different, in positive arrangement the concrete fills in the larger, and in negative arrangement the smaller rib. In the experimental programme, both arrangements are investigated, as it is shown in Fig. 3.

Table 2 Design characteristics of test specimens

No.	*Specimen*	P_{max} *[kN]*	P_{Rk} *[kN]*	P_{Rd} *[kN]*	P_{SLS} *[kN]*	*Secant stiffness [kN/m]*	*Displ. capacity [mm]*	*Failure mode*
1	SDn-1-s5	5,307	3,980	3,184	2,229	4500	3..6	1/a
2	SDn-1-s7	5,871	4,403	3,523	2,466	n.a.	n.a.	1/a
3	SDi-1-30-s7	9,107	6,830	5,464	3,825	7400	< 3	1/b
4	SDi-2-30-s7	12,517	9,388	7,510	5,257	7400	< 3	3/a
5	HSp-1-30-s5	7,546	5,660	4,528	3,169	7700	< 3	2/a
6	HSp-1-30-s7	7,186	5,390	4,312	3,018	15500	< 3	2/a
7	HSp-1-45-s5	7,588	5,691	4,553	3,187	17000	< 3	2/a
8	HSp-1-60-s5	7,575	5,681	4,545	3,182	n.a.	n.a.	2/a
9	HSp-2-30-s5	12,45	9,338	7,470	5,229	16400	< 3	2/a
10	HSp-2-60-s5	16,494	12,371	9,896	6,927	16200	3..6	2/b
11	SXCp-1-45-s5	10,053	7,540	6,032	4,222	14600	3..6	2/b
12	SXCp-1-55-s5	10,614	7,961	6,368	4,458	25000	3..6	2/b
13	EJ-1-t1.5-sp	6,489	4,867	3,894	2,726	7200	3..6	3/a
14	EJ-1-t1.5-sn	4,882	3,662	2,930	2,051	5100	< 3	3/a
15	EJ-2-t1.5-sp	11,472	8,604	6,883	4,818	8800	< 3	2/b
16	EJ-2-t1.5-sn	8,235	6,1763	4,941	3,459	8800	< 3	3/a
17	EJ-1-t2.0-sp	6,614	4,961	3,969	2,778	6500	< 3	3/a
18	EJ-1-t2.0-sn	6,584	4,938	3,950	2,765	3900	3..6	3/a
19	EJ-2-t2.0-sp	11,054	8,2905	6,632	4,643	8500	n.a.	3/a
20	EJ-2-t2.0-sn	7,993	5,9948	4,796	3,357	6000	< 3	3/a
21	EJ-1-t2.5-sp	8,075	6,056	4,845	3,391	6000	3..6	3/a
22	EJ-1-t2.5-sn	5,483	4,112	3,287	2,303	5400	< 3	3/a
23	EJ-2-t2.5-sp	13,361	10,021	8,017	5,612	11500	< 3	3/a
24	EJ-2-t2.5-sn	8,429	6,3218	5,057	3,54	11500	< 3	3/a
25	EJ-1-t1.5-sp-rf	7,614	5,711	4,568	3,198	3500	over 6	2/b
26	EJ-1-t2.0-sp-rf	9,912	7,434	5,947	4,163	10000	over 6	2/b
27	EJ-1-t2.0-sn-rf	6,702	5,027	4,021	2,815	10000	over 6	2/c
28	EJ-1-t2.5-sp-rf	13,008	9,756	7,805	5,463	8000	over 6	3/b
29	SX-1-t2.0-sp-rf	12,21	9,158	7,326	5,128	12000	over 6	1/c and 3/b
30	SX-2-t2.0-sp-rf	19,056	14,292	11,434	8,004	9400	over 6	1/c and 3/b

Three different types of fastening mode of screw are studied:

1. Normal fastening, when the self-drilling screw is drilled in standard way, fully into the sheets and the flange of the C-profile (applied in 2 specimens).
2. Inverse fastening, when the screw is drilled from inside of the flange so that only the threaded part of the screw is embedded in the concrete (2 specimens).
3. Partial drilling, when a part of the screw and the head are in the concrete (38 specimens).

The research focuses on the partial drilling which is analogous to the welded headed stud in composite structures with hot rolled steel sections. The applied embedment length ranges from 30 to 60 mm, as Table 1 shows. The used connector elements are the follows: three products of standard self-drilling screw - SFS SD6-6.3, HS-6.3, EJOT-JT2-6.3 - and a special product SFS SXC5-5.5, which is generally applied for sandwich panels and developed for large slip capacity between the supporting structure and the panel (SFS Stadler 2004).

The applied nominal thicknesses of C-profile are 1,5; 2,0 and 2,5 mm, the height is 200 mm in every specimen. A normal quality concrete block (C16) of 50 mm thickness above the rib is applied in all cases. In the last 12 specimens (which are tested in parallel with the pertinent full-scale beams) reinforcement of ϕ3,6/100 are used.

In the tests the load is applied by hydraulic jack. The relative displacement is measured between the flanges of the C-profile and the base plate (the longitudinal deformation of the concrete is neglected). The measured load and displacement data are collected and monitored by the computer controlled measurement system.

3.2 Test results

3.2.1 Observed behaviour and failure modes

On the basis of the experimental observations the following behaviour and failure modes are identified (Figs. 4 and 5):

3.2.1.1 Pull-out failures

Three basically different types of pull-out failure modes are observed, as it is shown in Fig. 4. *Pull-out and pull-over failure* (mode 1/a) occurs when the common beam-to-sheet connection is applied. Since only the head of the screw is embedded, under relatively low force level the head pulls-out from the concrete. The stiffness and the maximum load are low comparing to the other modes, and the ultimate strength is approximately equivalent to the ultimate shear force of the beam-to-sheet connection without concrete. The dominancy of the steel components appears in the descending branch of the behaviour: after the ultimate load is reached, a plastic zone appears in the plates and the pull-over failure occurs. The typical load-displacement curves of failure mode 1/a can be seen in Fig. 5.

Pull-out of the screw from the concrete (mode 1/b) is observed when the strength of the concrete is sufficient but the embedment is not effective: due to the relative slip the screw rotates and pulls out from the concrete. It is experienced in the case of the “inverse” fastening, when only the threaded part of the screw is placed into the concrete.

The third type of the pull-out failure is when the fastener pulls out from the flanges (mode 1/c). It occurs when the displacement capacity of the screw is large enough and the relative displacement between the concrete deck and the flanges is sufficient. Under these conditions the screw rotates and becomes more and more tensioned. If the displacement capacity of the screw is large enough, the screw can pull out from

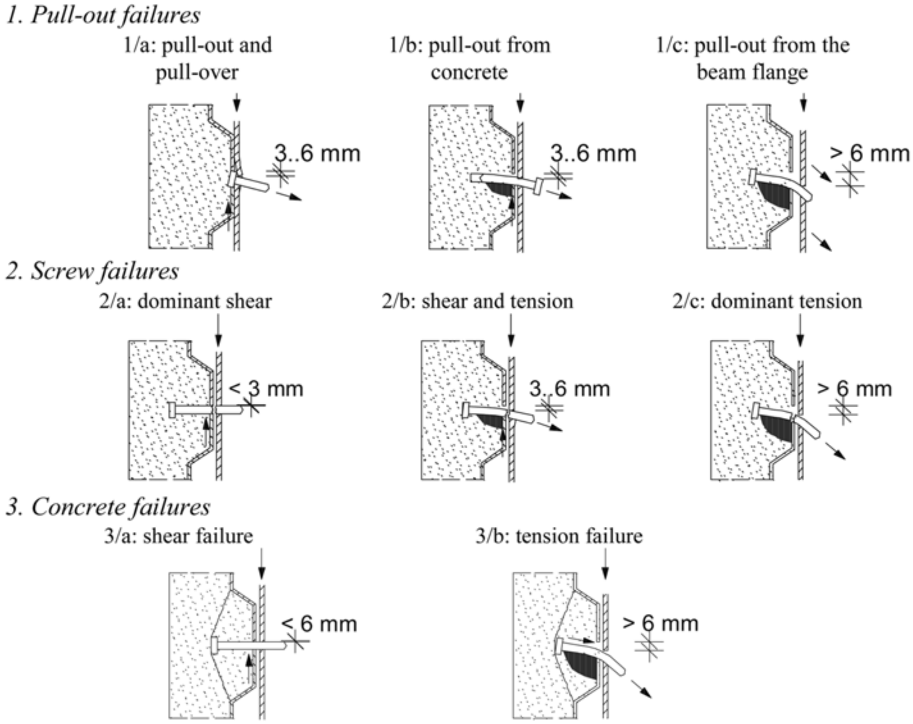

Fig. 4 Failure modes of composite connection

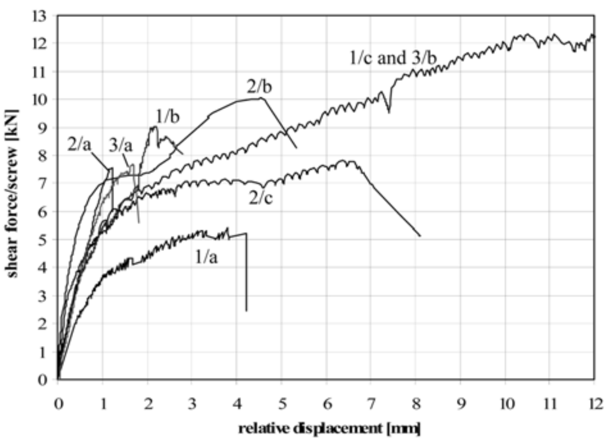

Fig. 5 Typical load-displacement curves of different failure modes

the flanges before the failure of the screw or the concrete, as it is shown in the pertinent curve of Fig. 5.

3.2.1.2 Screw failures

This phenomenon is similar to the described behaviour in failure mode 1/c, but the head of the screw provide the anchorage of the connector into the concrete. If the embedment is effective and the strength of the concrete is high enough, the screw fails by shear (mode 2/a), or by the combination of shear and tension (mode 2/b) or in extreme case under dominant tension (mode 2/c), depending on the relative displacement capacity of the connection. The differences between these three modes are well illustrated by the load-displacement curves of Fig. 5.

3.2.1.3 Concrete failures

Concrete failure occurs when the anchoring length of the screw is effective and the strength of the screw is relatively higher than the strength of the concrete. The failure depends on the direction of the transmitted force - similarly to the previous failure modes -, which can be concrete shear (mode 3/a) or tension of the concrete deck (mode 3/b) failure. The pertinent typical load-displacement diagrams are shown in Fig. 5, where the difference between the relative displacement capacities for the two modes can also be seen.

Fig. 6 shows the typical surfaces of the concrete after failure. It is influenced by the rib form (positive or negative fastening), the existence of reinforcement and the failure mode (shear or tension). In the specimens of Fig. 6/a - negative fastening of sheeting, no reinforcement - the crack surface is a typical cone with about 45 degrees. Fig. 6/b shows a typical failure surface when the width of the rib is larger so it behaves as a plane deck without rib; the failure mode is screw shear with a longitudinal crack and narrow crack cone. Fig. 6/c shows the concrete with the same dimensions but applying more ductile shear connector and reinforcement: the failure is caused by the tension of the screw that results in large extension of crack cone without longitudinal shear crack.

3.2.2 Investigation of connection parameters

The load-displacement curves of Fig. 7 illustrate the effect of the changing of connection parameters on the behaviour. The curves of Fig. 7/a belong to the same connection geometry (LTP20 sheeting in positive arrangement, EJOT screw with 35 mm embedment, reinforced concrete) but the thicknesses of the C-profile are different. By increasing of the thickness of the profile the stiffness and the resistance of the connection are significantly increased, due to the improved anchoring of the screws.

The curves in Fig. 7/b show the effect of other parameters: the arrangement of sheeting, the two-line fastening and the existence of reinforcement. In the studied four specimens the nominal thickness of the

(a) (b) (c)

Fig. 6 Different failure surfaces of the concrete deck

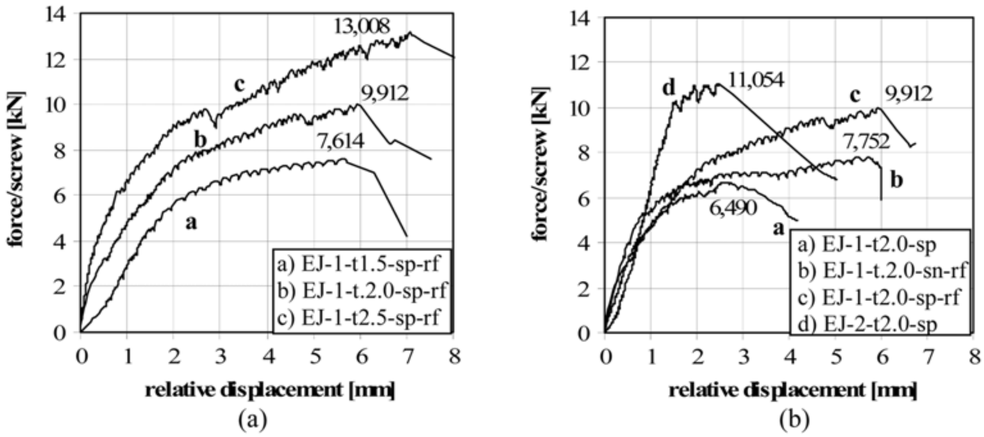

Fig 7 Load-displacement diagrams of push-out specimens: a) effect of plate thickness, b) effect of other structural parameters: fastening mode of sheeting, reinforced deck

C-profile is 2,0 mm, LTP20 sheeting and EJOT screw with 35 mm embedment are used. Curves *a* and *c* belong to specimens with positive trapezoidal sheeting arrangement and one line fastening, but in case *a* without reinforcement; it can be seen that the stiffness is practically the same but the difference is significant in resistance and displacement capacity. Curve *b* belongs to the same specimen with negative trapezoidal sheeting arrangement (with reinforcement). It can be also seen that the stiffness is practically the same but the ultimate behaviour and load are significantly different comparing to the equivalent specimens with positive sheet arrangement (curves *b* and *c*). Curve *d* in Fig. 7/b belongs to the specimen with two-line fastening (positive sheeting arrangement, without reinforcement): it shows similar stiffness and linear behaviour almost up to the ultimate load and lower displacement capacity.

Fig. 8 shows the difference between the specimens' behaviour when different screws are used. The load-displacement diagrams belong to the same specimen a) with the normal self-drilling screw, and b) with special SFS SXC5 screw. The two curves are quite similar in the initial part but the specimen with 'normal' screw (curve *a*) fails under a significantly smaller (24% reduced) load level, and having about

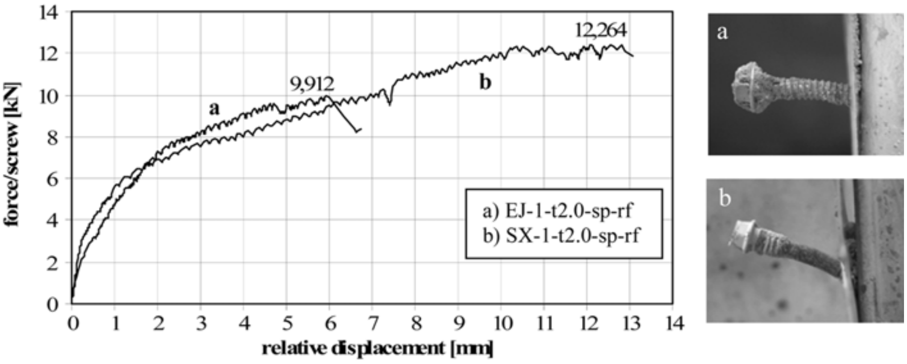

Fig. 8 Load-displacement diagrams of equivalent specimens with different shear connector

half of the displacement capacity than the specimen with SXC screw (curve *b*). In the first case (curve *a*) the failure mode is screw tension (mode 2/c), and in the second case (curve *b*) the combination of pull-out of the screw (mode 1/c) and concrete tension (mode 3/b) failures. The observed phenomena can be well illustrated by the deformation of the screws in Fig. 8.

3.2.3 Test based design values

On the basis of the Eurocode 4 and Eurocode 3 recommendations, the test based design resistance of the connection can be determined by Eq. (1):

$$P_{Rd} = (f_u/f_{ut})\frac{P_{Rk}}{\gamma_{Mv}} \tag{1}$$

where P_{Rk} the characteristics resistance, should be taken as the 90% of the failure load $P_{fail.min}$, divided by the number of connectors,

f_u the minimum specified ultimate strength of the connector's material,
f_{ut} the actual ultimate strength of the connector's material in the specimen,
γ_{Mv} = 1,25 the partial factor.

In the lack of accurate measuring possibility, approximate values of f_u/f_{ut} are applied for the combined "steel-concrete connector" between 0,8 and 0,85, consequently the design resistance of the connection is given by Eq. (2):

$$P_{Rd} = 0{,}75 \cdot P_{fail,min}/\gamma_{Mv} \tag{2}$$

On the basis of Wang's proposal (1998) the force level belonging to the serviceability limit state (SLS) can be calculated by the 50% of the measured minimum failure load. In the authors proposal the service load level is given by the 70% of the design resistance that means the 42% of the measured minimum failure load. The stiffness is given by a secant stiffness of the load-displacement diagram belongs to SLS value of the load, as it is shown in Fig. 9.

The design characteristics: the connection resistance, the initial stiffness and the relative slip capacity of the studied connections are summarized in Table 2.

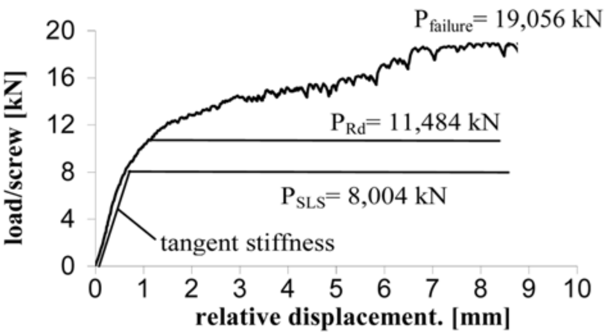

Fig. 9 Test based design values

3.2.4 Evaluation of the design values

3.2.4.1 Stiffness

From the evaluated results it can be seen that the stiffness depends mainly on the concrete behaviour and the thickness of the C-profile, as it is explained in Section 3.2.2. The determined initial stiffness ranges from 4500 to 25000 kN/m, as Table 2 shows.

The lowest stiffness belongs to the "normal" beam-to-sheet connection (specimen No. 1), when the trapezoidal sheeting is fastened in a common way to the top flange of the C-profile.

In case of specimens Nos. 25-30 with reinforced concrete, the thickness of the C-profile is the main component in the initial behaviour of the connection, as curve *a* in Fig. 7 shows. It means that the 'plastic' behaviour can be developed in the concrete and the fixing conditions of the connector - influenced by the flanges thickness - become dominant. The diagrams of Fig. 7 prove also the dominancy of steel flange properties: the other parameters such as the fastening mode of the sheeting and the applied number of the connector in a rib have minor affect on the stiffness.

3.2.4.2 Resistance

The resistances of the connections ranges from 3,18 to 7,81 kN in case of one line, and 4,94 to 11,43 kN in case of two-line-connection, as Table 2 shows. The ultimate behaviour and the resistance are influenced by the connection parameters: the fastening mode, the embedment length and the fastening line of the screw; the sheeting arrangement, the thickness of the C-profile and the material properties.

3.2.4.3 Ductility

In accordance with the recommendations of Eurocode 4 if the relative displacement capacity of the connection is 6 mm at least, it can be referred as ductile and the plastic design method can be applied in the design. Consequently in the classification of the subjected connections, each failure mode should be characterized based on the observed relative displacement capacity, too.

In case of shear failure modes (screw shear 2/a and concrete shear 3/a in Fig. 4) the relative displacement capacity of the connections is under 3 mm.

When the slip capacity does not reach the required 6 mm, medium displacement capacity is defined between 3 and 6 mm. Pull-out and pull-over failure (1/a in Fig. 4), combination of screw shear and tension failure (2/b in Fig. 4) and concrete shear failure in each cases (specimens Nos. 13, 16 and 17) belong to this group.

The specimens that characterized by dominant tension failures (1/c, 2/c, 3/b in Fig. 4) show the required displacement capacity at least 6 mm. These failure modes are observed in specimens with reinforced concrete (Nos. 25-30). The most favourable behaviour in the full test program is observed in case of SXC screw shear connectors: the measured app. 12 mm relative slip capacity highly exceeds the 6 mm limit value, as it is illustrated in Fig. 8.

Based on the observed ductile behaviour the specimens belonging to dominant tension failure are proposed in floor application.

4. Full-scale composite beam tests

4.1 Experimental programme

Six full-scale beam specimens are investigated with the same global parameters as follows: 5,980 mm span, C-profile with 200 mm height, LTP20 trapezoidal sheeting, and concrete deck of 50 mm thickness above the rib with normal quality (C16/20). The following parameters are modified: the thickness of the C-profile (1,5...2,5 mm), the type of connector element (EJOT-JT2-6.3 and SXC5-5.5) and the arrangement of the trapezoidal sheet (positive and negative), as it is shown in Table 3. The applied parameters are based on the proposed geometry of the developed floor system (EJOT-JT2 screw with partially drilling, positive trapezoidal sheeting arrangement and 2,0 mm nominal plate thickness of the C-profile) and the observed favourable behaviour in push-out tests (SXC screw). The inverse fastening of sheeting is studied only with the most common, 2,0 mm thickness of the C-profile (specimen No. 3).

The span of the specimens is chosen to reach the full composite action in the middle cross-section considering the measured shear resistance of a single connector. A four-point-bending arrangement is applied in the tests with two concentrated loads 800 mm from each other.

The specimens are built by two C-profiles (with 600 mm distance) and the attached concrete deck (with 1,200 mm width), as Fig. 10 shows. This arrangement provides the uniform load distribution between the beams, and ensures the parallel measuring in the beams. To avoid the torsion of the lower

Table 3 Geometrical parameters of the full-scale beam specimens

Specimen	***L [mm]***	***d_{beam} [mm]***	***C-profile***	***Sheet***	***Screw type***	***Emb. length [mm]***	***Screw line***
			height-thickness	***height-thickess.-arrangement***			
1. FN-15-EJ	5980	600	C200-1.5	LTP20-0.5 pos.	EJOT JT2-6.3	35	1
2. FN-20-EJ			C200-2.0	LTP20-0.5 pos.	EJOT JT2-6.3	35	1
3. FI-20-EJ			C200-2.0	LTP20-0.5 neg	EJOT JT2-6.3	35	1
4. FN-25-EJ			C200-2.5	LTP20-0.5 pos.	EJOT JT2-6.3	35	1
5. FN-20-SX1			C200-2.0	LTP20-0.5 pos.	SXC5-5.5	45	1
6. FN-20-SX2			C200-2.0	LTP20-0.5 pos.	SXC5-5.5	45	2

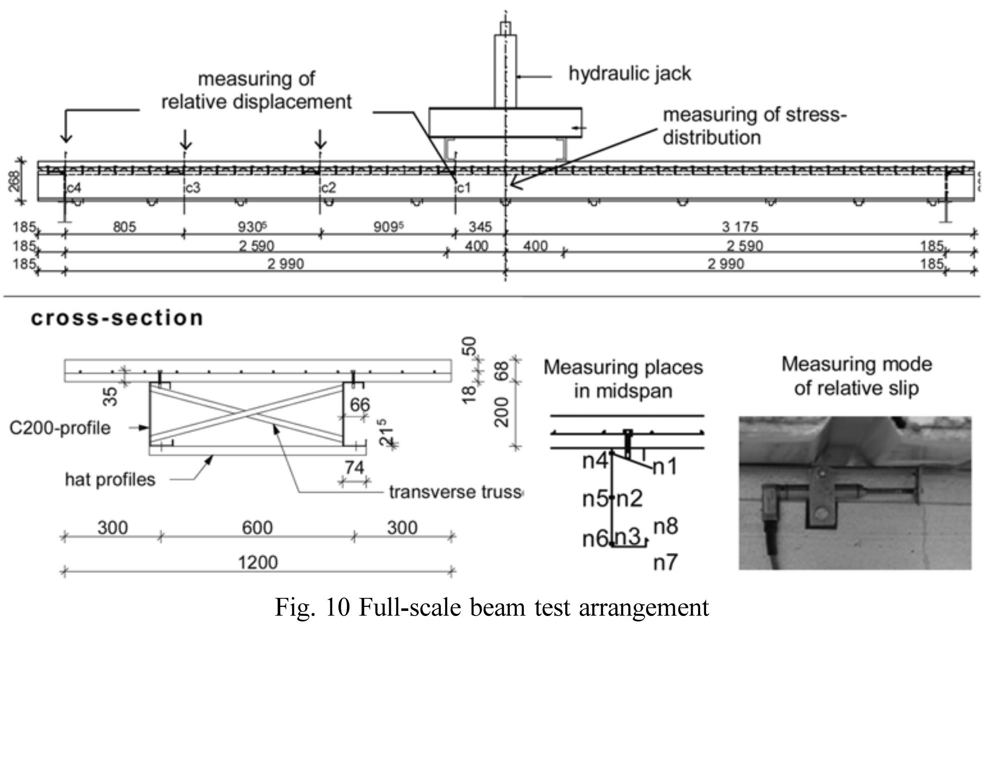

Fig. 10 Full-scale beam test arrangement

flange and to prevent the lateral instability a bracing system is used: the bottom flanges are joined by hat profiles and transverse trusses are applied in three cross-sections along the beam, as it is shown in Figure 10.

In the test arrangement two concentrated loads are applied by a hydraulic jack. The measured values: the load, the maximum displacements, the relative displacements between the upper flange of the C-profile and the concrete deck, and the stress distribution in the C-profiles in the mid-span. The measurement system of relative displacement is shown in Fig. 10. The strain gauges in the mid-span are installed on both side of the web and in the bottom flanges, as Fig. 10 illustrates.

4.2. Experimental results

4.2.1 Load-deflection relationship

Table 4 shows the measured mid-span deflection and the equivalent load values under a low, 1 kN load level, and under the load level belonging to serviceability limit state with the applied L/300 deflection limit (SLS load).

The initial stiffness and the elastic behaviour are investigated by the structural response under 1 kN load/beam level. The measured maximum displacement $e_{1kN.test}$ ranges from 1,03 to 1,56 mm, as shown in Table 4. On the basis of Veljkovic and Johansson (2006) the acceptable dynamic behaviour for a floor structure is reached if the maximum deflection caused by 1 kN concentrated load remains under 1 mm. Although the tested specimens are not designed for this requirement, the data are enclosed for information on the initial stiffness. The measured values are compared to the calculated mid-span deflections $e_{1kN.calc}$, using ideal cross-section assuming rigid shear connection and the differential equation of elastic beam. The comparison of the two values shows the effect of the stiffness of the shear connection: the ratio of the calculated and the measured deflections ranges from 0,91 to 0,95 that shows significant initial stiffness.

The ratio of the measured ($F_{L/300.test}$) and the calculated value with rigid shear connection ($F_{L/300.full}$) ranges from 0,69 to 0,77 in the load level belonging to serviceability limit state (L/300 deflection). The lower structural stiffness shows the nonlinear behaviour of the shear connection at SLS load level.

The curves in Fig. 11 show the load - mid-span deflection relationship of the beam specimens. In Fig. 11/a the curves belong to the specimens with the same shear connection with different thicknesses of the C-profile, and in the case of 2,0 mm nominal thickness the fastening mode of the sheet is changed (Nos. 1-4 in Table 3). In Fig. 11/b the load-displacement diagrams of specimens with SXC5-5.5 screws are shown (one-and two-line-connection, Nos. 5-6).

Table 4 Deflections of the specimens

Specimen	1 kN load			SLS (e = 19,93 mm)		
	$e_{1kN.full}$ full interaction [mm]	$e_{1kN.test}$ [mm]	$e_{1kN.full}$/ $e_{1kN.test}$	$F_{L/300.full}$ full interaction[kN]	$F_{L/300.test}$ [kN]	$F_{L/300.full}$/ $F_{L/300.test}$
1. FN-15-EJ	1,415	1,56	0,91	14,089	9,760	0,69
2. FN-20-EJ	1,126	1,19	0,95	17,710	13,650	0,77
3. FI-20-EJ	1,131	1,22	0,93	17,630	13,000	0,74
4. FN-25-EJ	0,946	1,03	0,92	21,067	15,804	0,75
5. FN-20-SX1	1,126	1,19	0,95	17,710	12,450	0,70
6. FN-20-SX2	1,126	1,19	0,95	17,710	13,530	0,76

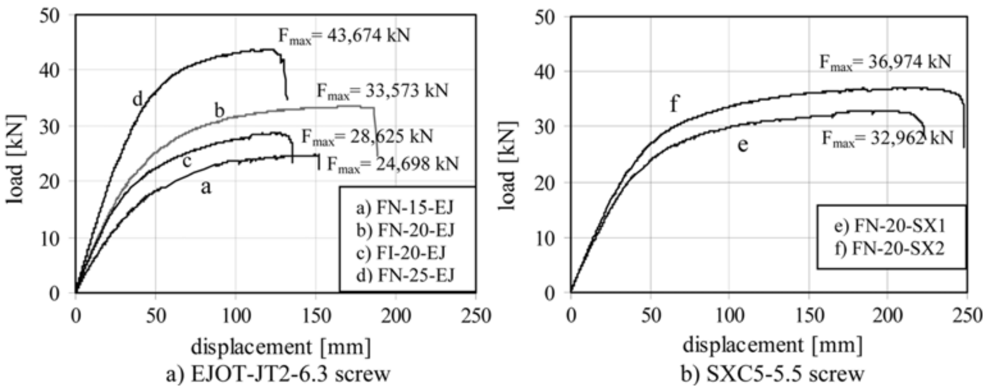

Fig. 11 Load-displacement diagrams of full-scale beam specimens

On the basis of the load-displacement diagrams it can be stated that the behaviour of the specimens are practically linear until about the 50% of the maximum load. The effect of the sheet fastening (curves *b* and *c*) and the effect of the one- or two-line-connection (curves *e* and *f*) are not significant until the nonlinear range is reached (as it is observed in the push-out tests, too).

The maximum loads are between 24,70 kN and 43,67 kN; the maximum load to SLS load ratio ranges from 2,20 to 2,76. The ratio of the highest and lowest maximum load value is 1,77. The behaviour of the specimen with positive sheet fastening is favourable: the difference between the equivalent specimens with positive and negative sheet fastening is 17% in the maximum load, and 38% in the maximum displacement (curves *b* and *c*). On the basis of the load-displacement diagrams, the effect of one- or two-line-connection is not significant: the resistance of the FN-20-SX2 specimen (curve *f*) is only 12% higher than the resistance of FN-20-SX2 specimen (curve *e*).

The specimens FN-20-EJ, FN-20-SX1 and FN-20-SX2 show the most favourable plastic behaviour with large displacement capacity. The other specimens show also reasonable ductility. The maximum displacements range from 150 to 240 mm (L/46...L/24); the highest displacement capacity is measured in case of FN-20-SX2 specimen (curve *f*). The large deflection of the specimen can be seen in Fig. 12.

4.2.2 Failure modes

During the tests two different types of ultimate behaviour are observed: a) the failure of the screw,

Fig. 12 Deflection of test specimen FN-20-SX2 at collapse state

and b) the plastic bending failure of the composite beam.

4.2.2.1 Screw failure

As it is explained in the push-out test programme when the displacement capacity of the screw connector is not enough to carry the relative displacement between the top flange of the C-profile and the concrete deck, screw failure is occurred. It is observed in specimens with EJOT screws (specimens Nos. 1-4). The load - midspan displacement diagrams of these specimens are shown in Fig. 11/a. In case of inverse fastening of sheet (FI-20-EJ), the concrete deck is separated from the sheeting after the screws are failed, due to the smaller rib dimensions, as Fig. 13/a illustrates. After the composite action is vanished the total load is transmitted to the C-profiles causing a sudden failure of the compressed zone by local buckling, as illustrated in Figs. 13/a and b.

4.2.2.2 Bending failure

The specimens FN-20-SXC1 and FN-20-SXC2 show basically different behaviour in ultimate limit state: plastic hinges appear in the cross-sections of the concentrated loads, and the final failure is occurred by dominant bending, as shown in Fig. 13/c. The large strains in the lower flange lead to the fracture in the net cross-section (where the fastened hat profile of the lateral bracing is connected), as Fig. 13/d shows. This observed behaviour is a favourable mode and it is aimed to be reached by proper design during practical application.

4.2.3 Relative displacement

Fig. 14 summarizes the load-relative slip relationships of beam specimens with $t_{nom} = 2{,}0$ mm thickness of the C-profile. From the curves it can be seen that the shear connections undergo plastic

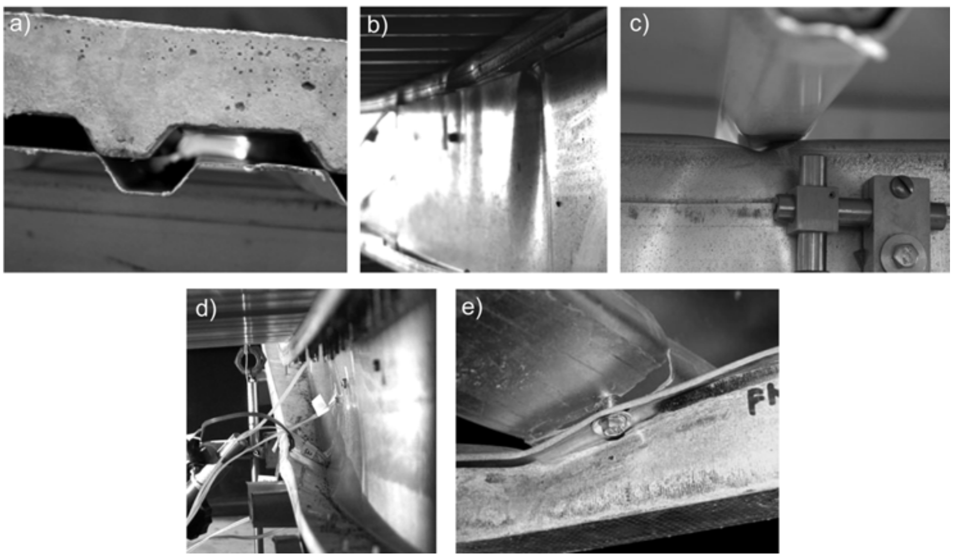

Fig. 13 Examples of ultimate behaviour: a) screw failure and uplift of concrete deck, b) and c) buckling of specimen FI-20-EJ after the failure, d) plastic bending failure of the beam with SXC screw, e) tension fracture of the bottom flange

(a)

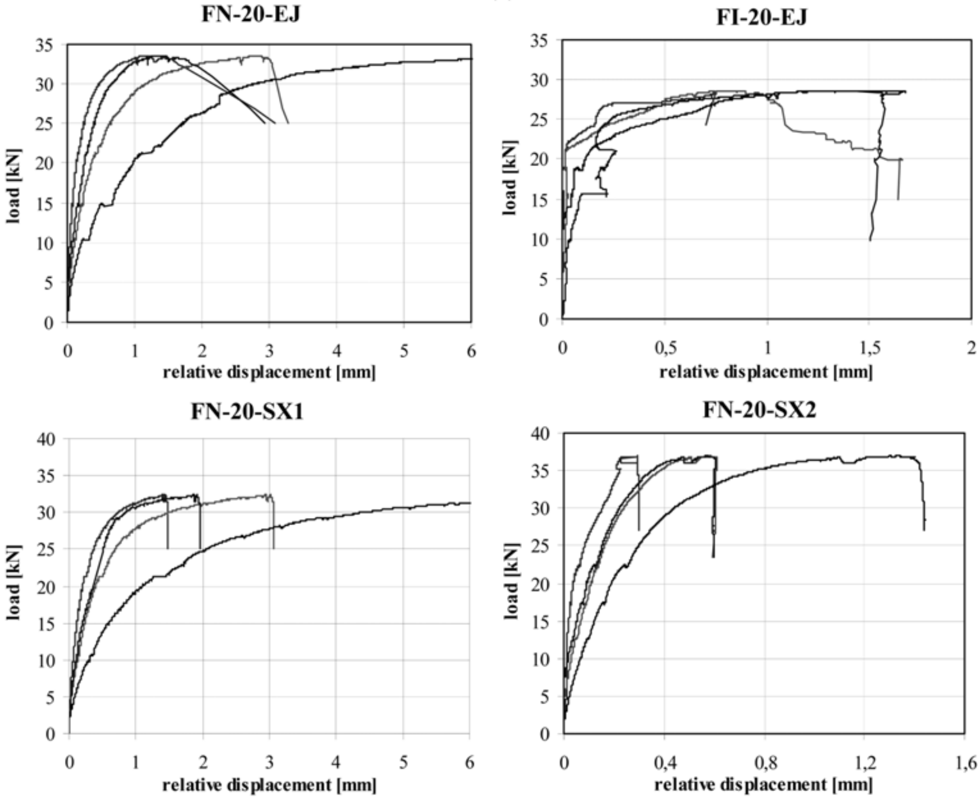

(b)

Fig. 14 a) Rotation of the screws due to relative displacement b) load - relative displacement diagram of equivalent specimens with different shear connections

state in a relatively low 1-2 mm mean slip level. The final slip belongs to failure remains under the measured slip capacity in push-out specimens (see Fig. 7). In FI-20-EJ specimens the behaviour is rather rigid-plastic, as Fig. 14 shows and the observed buckling after the ultimate load is reached, presented in Section 3.5.2, is shown in the descending branch of the load-relative slip curves.

In the tests it is proved that the plastic slip is developed in all specimen, what is the requirement of the developed design method (Dunai, *et al.* 2003/b).

4.2.4 Stress distribution

The stress in a given point can be determined from the measured strain and the belonging stress values

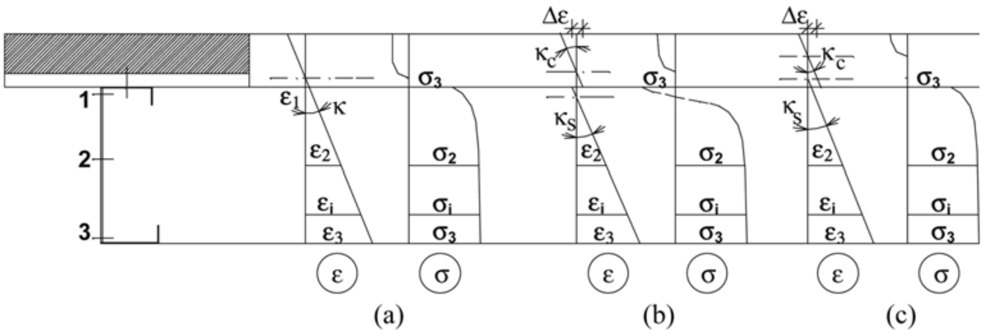

Fig. 15 Stress distribution in the cross-section under positive bending: a) rigid shear connection; b) semi-rigid shear connection, neutral axis of steel in the web, c) semi-rigid shear connection, neutral axis of steel in the concrete deck

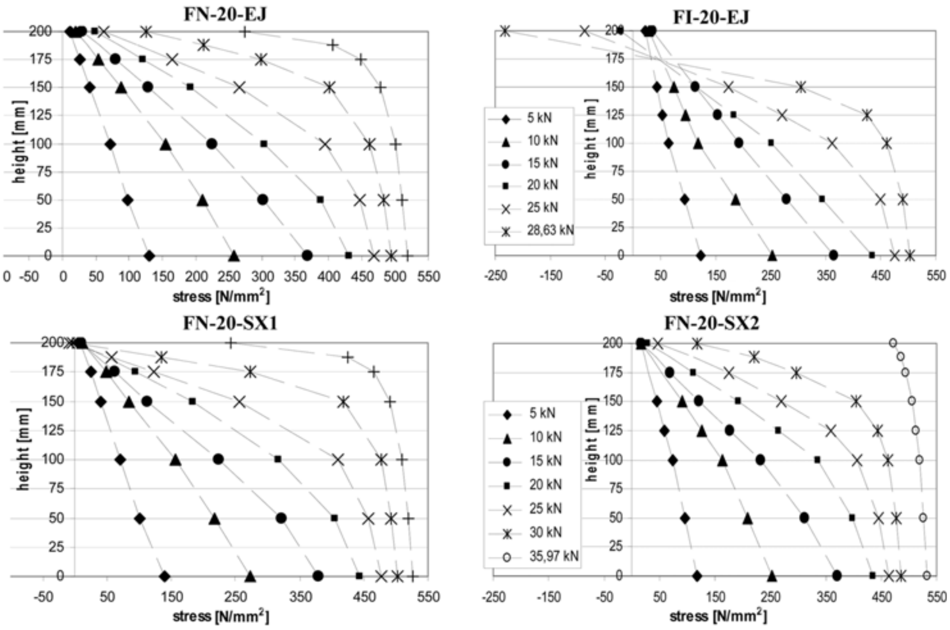

Fig. 16 Stress distribution in the mid-span in equivalent full scale beam specimens with different shear connection

from the stress-strain relationship of the component material. In full-scale beam specimens the load-strain distribution is measured in the middle cross-section of the C-profile, as it is shown in Fig. 10.

Fig. 15 shows the behaviour of a composite cross-section under positive bending. Fig. 15/a shows the rotation of the cross-section and the nonlinear stress distribution when the steel and concrete parts act together and the neutral axis is in the concrete deck (rigid shear connection).

If the shear connection is semi-rigid, relative slip occurs and the rotation of the steel and concrete cross-sections occurs separately depending on the degree of composite action. The neutral axes of steel and concrete parts become also separated, but it is assumed that the hypothesis of plane cross-sections remains valid for the components. Fig. 15/b illustrates the possible strain and stress distribution when the neutral axis of steel is in the steel section near the top flange and a small part of the upper section is compressed. Fig. 15/c shows the case when the neutral axes both of the steel and concrete section are situated in the concrete deck and the whole C-section is tensioned.

The changing of the stress distribution in the web of the C-profile under the increasing loading is shown in Fig. 16. The strains are measured in three places in the web: at the top and bottom flanges and in the middle point as Fig. 10 shows. In internal places linear approximation is applied for the strains and the stress in the actual point can be determined based on the measured stress-strain relationship of the steel material.

As Fig. 16 shows the stress distribution is linear elastic in the beginning of the loading process. In accordance with the behaviour of a bended cross-section, the plastic yielding appears first in the bottom part and under increasing loads it extends to the upper parts of the cross-section. The stress distribution in a given load level depends on the position of the neutral axis in a composite cross-section that is determined by the geometry of the components and the degree of composite action.

The specimen with the same thickness of C-profile and sheeting arrangement, but different shear connection (FN-20-EJ, FN-20-SX1 and FN-20-SX2) show quite the same stress-distribution at ultimate loading level. In FI-20-EJ specimen (inverse fastening of sheeting) the top flange is tensioned until about the 50% of the maximum load is reached. After the plasticity develops the force distribution is changed and the upper part of the C-section becomes compressed.

On the basis of the observed stress distributions it can be concluded that the plastic behaviour develops in the thin-walled C-profile therefore the plastic design recommendations of Eurocode 4 for the composite cross-section can be applied if the local buckling of compressed part of the cross-section is considered.

5. Summary and conclusions

A new type of light-gauge composite floor system is investigated by an extended experimental study. The results and conclusions are summarized as follows:

In the first step of the research an experimental parametric study is completed to determine the behaviour of the screwed shear connection by applying push-out tests. The efficiency of the different arrangements and the effect of connection parameters are studied. On the basis of the observed failure modes, the behaviour is characterised and classified and the design values of the stiffness, resistance and ductility are calculated and evaluated. It can be stated that the connections that show tension type failure modes result in significant relative displacement capacity. The measured connection stiffness is low and should be considered in the design.

In the next step of the experimental study full-scale beam tests are completed using the most efficient shear connection arrangements obtained from the push-out tests. Detailed measuring is concentrated on the global stiffness, the composite action and the stress distribution. In the investigation of the global ultimate behaviour it is concluded that the floor beams with the most ductile shear connections have the most favourable behaviour with plastic bending failure of the beam. The developing of the plastic zones in the steel cross-sections and the plastic deformation of the shear connection confirm the applicability of partial shear connection based plastic design method for the developed composite beam.

Acknowledgement

The research work is conducted under the financial support of the OTKA T035147 project and OM ALK00074/2000 R&D project in the co-operation of BME and Lindab Ltd.

References

Building Works, Inc. (2003), "Prescriptive method for connecting cold-formed steel framing to insulating concrete form walls in residential construction", Report, Cambridge, UK.

Dunai, L., Ádány, S., Erdélyi, S. and Petrasko, R. (2003/a), "Development of Lindab Floor System, Design manual and design tables", R & D Report, BME, 13/II, Budapest, Hungary (in Hungarian).

Dunai, L., Erdélyi, S. and Ádány, S. (2003/b), "Design method of light-gauge composite floor beam", *Proc. of Int. Conf. on Advances in Structures, Steel, Concrete, Composite and Aluminium*, Sydney, Australia, 317-323.

Earl Composite Systems (2001), "MetalStudCrete (MSC) - shear transfer strip", Report, Irwindale, California, USA.

Erdélyi, S. (2007), "Light-gauge steel and concrete composite beams", PhD Dissertation.

Erdélyi, S. and Dunai, L. (2002), "Experimental study on connection of composite light-gauge floor system", *Proc. of 3rd European Conf. on Steel Structures*, Coimbra, Portugal, 441-450.

Erdélyi, S. and Dunai, L. (2004), "Behaviour of a new type of composite connection", *Periodica Polytechnica Ser. Civ. Eng.*, **48**(1), 1-12.

Erdélyi, S. (2005), "Numerical simulation of the behaviour of light-gauge composite floor beam", *Proc. of 15th Inter, Institute Seminar*, Budapest, Hungary, 15.

Erdélyi, S. and Dunai, L. (2005), "Experimental investigation of composite light-gauge floor beams", *Proc. of 4rd European Conf. on Steel and Composite Structures*, Maastricht, The Netherlands, Vol. B., Chapter 4.3, 25-32.

ENV 1993-1-1 (1993), Eurocode 3, *Design rules for steel structures, Part 1-1, General rules and rules for buildings*.

ENV 1993-1-1 (1996), Eurocode 3, *Design rules for steel structures, Part 1-3, General rules and supplementary rules for cold-formed thin gauge members and sheetings*.

ENV 1994-1-1 (1999), Eurocode 4, *Design of Composite Steel and Concrete Structures, Part 1-1, General Rules and Rules for Buildings.*

Hanaor, A. (2000), "Tests of composite beams with cold-formed sections", *Int. J. Constr. Steel Res.,* **54**, 254-264.

Mujagic, J.R.U., Easterling, W.S. and Murray, T.M. (2001), "Standoff screws as shear connectors for composite trusses: push-out test results and analysis", *Proc. of the Int. Conf. on Connection between Steel and Concrete*, Stuttgart, Germany, 1240-1249.

Narayanan, R. (1988), *Steel-concrete composite structures - Stability and strength,* Elsevier Applied Science.

SFS Stadler, Ltd. (2004), *Technical performance values for SFS fasteners*, Marketing Documentation, Dortmund, Germany.

Veljkovic, M. and Johansson, B. (2006), "Light steel framing for residential buildings", *Thin-Wall. Struct.,* **44**(12), 1272-1279.

Wang, Y.C. (1998), "Deflection of steel-concrete composite beams with partial shear interaction", *J. Struct. Eng.* ASCE, **124**(10), 1159-1165.

DN